International Journal of Biological Macromolecules 313 (2025) 144285

Contents lists available at ScienceDirect

International Journal of Biological Macromolecules

journal homepage: www.elsevier.com/locate/ijbiomac

Biocontrol potential of *Vibrio maritimus* chitinase: Heterologous expression and insecticidal activity against *Acanthoscelides obtectus*

Neslihan Dikbaş [a,*], Ahmet Tülek [b], Sevda Uçar [c], Şeyma Alım [a], Burak Servili [d], Nurettin Paçal [b], Göksel Tozlu [e], Sezai Ercisli [f]

[a] *Ataturk University, Agricultural Faculty, Department of Agricultural Biotechnology, Erzurum, Turkey*
[b] *Iğdır University, Department of Bioengineeringand Sciences, Iğdır, Turkey*
[c] *Sivas Science and Technology University, Faculty of Agricultural Sciences and Technology, Department of Field Crops, Sivas, Turkey*
[d] *Kadir Has University, Graduate School of Science and Engineering, Bioinformatics and Genetics Program, Istanbul, Turkey*
[e] *Ataturk University, Agricultural Faculty, Department of Plant Protection, Erzurum, Turkey*
[f] *Ataturk University, Agricultural Faculty, Department of Horticulture, Erzurum, Turkey*

ARTICLE INFO

Keywords:
Vibrio maritimus
Chitinase
Acanthoscelides obtectus
Biopesticide
Molecular dynamics simulations

ABSTRACT

In this study, the chitinase gene from the marine bacterium *Vibrio maritimus* was heterologously expressed in *Escherichia coli*, purified via affinity chromatography and tested for its insecticidal activity against the storage pest *Acanthoscelides obtectus*. The recombinant *Vm*ChiA protein exhibited a molecular mass of ~60 kDa, with optimum activity observed at pH 6.0 and 40 °C. Enzyme kinetic analysis revealed a K_m value of 0.042 mM, V_{max} of 17.48 μmol min^{-1}, k_{cat} of 1.75 min^{-1} and catalytic efficiency of 41.61 mM^{-1} min^{-1}, respectively. Furthermore, a dose of 40 U mL^{-1} of recombinant *Vm*ChiA showed similar efficacy to malathion insecticide against *A. obtectus*, with 100 % mortality in both treatments. LC_{50} and LC_{90} values of *Vm*ChiA were 13.95 U mL^{-1} and 27.66 U mL^{-1}, respectively. Furthermore, the three-dimensional structure of the catalytic site of *Vm*ChiA was modeled. Molecular dynamics simulation technique was used to explore and analyze the dynamics and interactions. A salt bridge (GLU274-ARG296) in the α + β domain was observed as a critical feature facilitating substrate $(GlcNAc)_2$ binding and enzymatic activity. These findings demonstrate that recombinant *Vm*ChiA possesses potent insecticidal properties, highlighting its potential as a bio-based, eco-friendly alternative for managing significant agricultural pests.

1. Introduction

Beans (*Phaseolus vulgaris* L.) are one of the legume plants that hold great importance in human nutrition due to their high content of protein, carbohydrates, vitamins, minerals and vegetable fibers [1]. Despite their socioeconomic importance, the production of this crop suffers great losses due to various diseases and pests [2]. Insect attacks account for the majority of losses in production and storage [3]. *Acanthoscelides obtectus* (Say) (Coleoptera: Chrysomelidae: Bruchine), also known as the bean seed beetle, is one of the most important and widespread pests causing significant losses in both wild and cultivated beans [4]. Pest infestation begins in the fields when females lay eggs on the pods and then spreads to storage facilities, causing the rapid destruction of bean seeds [5]. Larvae feeding inside the seeds cause deterioration in seed quality, poor germination, reduced nutritional and aesthetic value, and altered taste and flavor. Yield losses due to *A. obtectus* have been reported to range between 48 % and 100 % depending on storage conditions [6]. Synthetic pesticides (phosphine, pyrethroids, organophosphates, etc.) are generally used to minimize these losses and control the pest [7]. However, these pesticides disrupt the ecological balance, cause toxic effects onhumans and other living organisms, and lead to the develoment of pesticide resistant pest varieties [8]. These problems and limitations encourage the development of more sustainable and alternative strategies for pest control [9].

Biological control of pests by targeting chitin structures is a non-toxic, environmentally friendly method that does not promote insect resistance [10,11]. Indeed, chitin is an important polysaccharide found in the cuticle that forms the exoskeleton of insects, the peritrophic matrix (PM) lining the epithelium of the midgut, eggshells and muscle attachment points [12,13]. This compound is hydrolyzed by the enzyme

* Corresponding author.
E-mail address: neslidikbas@atauni.edu.tr (N. Dikbaş).

https://doi.org/10.1016/j.ijbiomac.2025.144285
Received 26 February 2025; Received in revised form 22 April 2025; Accepted 14 May 2025
Available online 16 May 2025
0141-8130/© 2025 Elsevier B.V. All rights are reserved, including those for text and data mining, AI training, and similar technologies.

chitinase which is extracted from many prokaryotic and eukaryotic organisms, and belongs to the family of glycoside hydrolases capable of hydrolyze β-(1,4) bonds in its structure [14]. Because of this property, chitinase enzyme is emerging as a potential biopesticide for pest control in agricultural production [11,15]. In order to optimize the use of chitinase in insect control, there is a strong interest in the cloning and characterization of the chitinase gene and the development of more efficient chitinase producing strains [16].

Chitinases (EC 3.2.1.14) break β-(1,4)-glyosidic bonds and degrade chitin by cleaving (GlcNAc)n longer fragments ($n > 1$) into monomers and/or oligomers [17]. Moreover, Chitinases are categorized as glycosyl hydrolase (GH) families GH18, GH19 and GH20 in the carbohydrate-active enzymes (CAZy) database [18,19] based on amino acid sequence and domain structure. GH19 family chitinases are frequently found in plants, while GH18 family chitinases are commonly found in almost all organisms [20]. Additionally, the GH18 chitinase family has been divided into many subgroups based on its definition in the literature [21]. Mainly, subgroup A contains the α + β insertion site in the catalytic domain of bacterial chitinase, which is absent in the other groups, B and C [22]. The α + β insertion site provides an open deep active binding cleft around the substrate binding site of the enzymes and enhances the processivity required for efficient degradation of long chitin oligomers [23,24].

V. maritimus chitinase (*Vm*ChiA) protein sequence (UniProtKB: A0A090T850, GenBank: GAL36101.1) was highly similar (sequence identity: 82.4 %) to the X-ray cyrstal three-dimensional monomeric structure of *V. harveyi* Chitinase A (*Vh*ChiA, PDB ID: 3ARR, Resolution: 1.65 Å) amino acid sequence [25]. The *Vh*ChiA structure consists of 3 domains, a N-terminal chitin-binding domain (between 22 and 138 residues), an $(\alpha/\beta)_8$ TIM-barrel catalytic domain (residues 159–588) and an α + β insertion domain (residues 461–547) [26]. Similarly, *Vm*ChiA structure has the same domains. Finally, *Vh*ChiA is thought to catalyze substrate hydrolysis by a "slide and bend mechanism". This mechanism consists of four steps. Substrate recognition, sliding and bending, bond cleavage and product release [27].

Molecular dynamics (MD) simulations are a computer simulation method that models the motion and interactions of molecules at the atomic level. The MD method is used to understand and analyze the dynamics of molecules [28]. Many MD studies of the chitinase enzyme have been performed and reported [29–32]. Previously, in the study by Segura-Cabrera et al. [29], the three-dimensional structure of the OvCHT1 (chitinase of *Onchocerca volvulus*) enzyme was predicted and closantel binding site was investigated in comparison with human chitinases [29]. Using molecular dynamics simulations and free energy calculations, the specific binding characteristics of closantel to OvCHT1 were determined (Arg35, Trp70, Asn295, Thr300) [29]. In a study, Jitonnom et al. [33] investigated the reaction mechanism in *Serratia marcescens* Chitinase B (*Sm*ChiB) enzyme. Based on the results, the neutral form of Asp142 was found to electrostatically stabilize the oxazolinium ion intermediate formed during the reaction and this form was preferred for the reaction. Furthermore, Tyr214 was shown to play a critical role for the reaction, especially in the deglycosylation step [33]. In another study by Khan et al. [30], structural analyses and molecular docking studies showed that the amino acid Glu176 is critical for enzyme activity. The three-dimensional structure of the enzyme (Thermomyces lanuginosus SSBP chitinase II) was predicted by homology modeling and ab initio methods and reported to have a TIM-barrel structure [30]. In another study, Khan et al. [32] determined the optimum activity and stability conditions of Chitinase I enzyme from *Thermomyces lanuginosus* SSBP. Simulations showed that the enzyme maintained its structural stability in the temperature range of 300–375 K. Furthermore, pH-dependent molecular dynamics simulations showed that the enzyme retained its characteristic TIM-barrel structure at low pH values [32]. The objective of the aforementioned investigation, whether pertaining to various chitinase subgroups or to the chitinase enzyme of different organisms, is to understand the relationships and dynamics of chitinase structure.

Recombinant protein production in *Escherichia coli* is widely employed due to its high yield, rapid growth, low production costs compared to eukaryotic systems, and short production timelines [34], despite disadvantages such as contaminating endotoxins, foldind problems, and the lack of eukaryotic post-translational modifications [35]. In this study, the chitinase gene from *V. maritimus* was cloned and expressed heterologously in *E. coli*. The protein sequence (UniProtKB: A0A090T850) of the *V. maritimus* chitinase (*Vm*ChiA) was obtained from the UniProt database [36]. However, the three-dimensional structure of *Vm*ChiA obtained from experimental studies, according to the amino acid sequence in UniProtKB: A0A090T850, was unavailable in UniProt and similar protein structure databases. Therefore, in silico methods were used to model the three-dimensional monomeric structure of the *Vm*ChiA catalytic domain based on the amino acid sequence. The structural differences, interactions and dynamics of *Vm*ChiA structure were investigated in the docked and undocked of $(GlcNAc)_2$ by molecular dynamics simulations method over 100 ns. Moreover the interactions of *Vm*ChiA with $(GlcNAc)_2$ at the ligand binding site were also investigated. In addition, the biochemical properties of purified *Vm*ChiA and its activity against *A. obtectus* were evaluated.

2. Material and Method

2.1. Gene cloning, heterologous expression, and purification

The chitinase gene from *V. maritimus* (UniProt accession number: A0A090T850, NCBI GenBank: BBMT01000009.1) was analyzed and synthesized using synthetic gene technology (Gene Universal, USA). The putative *V. maritimus* chitinase gene (*vmcht*), encoding a protein of 586 amino acids, was codon-optimized and cloned into the pET28a(+) plasmid at the *Nde*I and *Xho*I restriction sites. The pET28a(+)-vmcht plasmid was subsequently transformed into $CaCl_2$-competent *E. coli* BL21 cells [37]. Transformants were selected on LB-agar plates supplemented with kanamycin (50 mg mL^{-1}). For the expression of the *vmcht* gene, a single colony was inoculated into liquid LB medium containing kanamycin and incubated overnight at 37 °C, shaking at 5 RCF. The following day, 1 mL of the culture was transferred into 250 mL of fresh LB-kanamycin medium and incubated at 30 °C, shaking at 5 RCF. Upon reaching an OD_{600} of 0.45–0.55, isopropyl β-D-1-thiogalactopyranoside (IPTG) was added to a final concentration of 1 mM to induce gene expression, and the culture was incubated for an additional 5 h.

Following the expression process, the cell pellets obtained by centrifugation at 2632 RCF for 10 min at 4 °C were resuspended in lysis buffer (pH 8.0; 5 mM imidazole, 500 mM NaCl, and 20 mM sodium phosphate) at a ratio of 4 mL per gram of pellet, and subsequently placed on ice. Lysozyme was added to the cell suspension to a final concentration of 1 mg mL^{-1}, and the mixture was incubated on ice for 30 min. Post-incubation, the cells were subjected to sonication on ice with a cycle of 20 s on and 10 s off for a total duration of 4 min. The resulting homogenate was centrifuged at 10528 RCF for 1 h at 4 °C to remove cellular debris. The *Vm*ChiA proteins, which feature a C-terminal 6xHis-tag, were purified from the cell lysate using HisTrap FF (5 mL) columns via immobilized metal affinity chromatography (IMAC) on an AKTA Prime Plus Purification system. The system was initially washed with 5 column volumes of 20 % ethanol followed by ultra-pure water. The column was equilibrated with 5 column volumes of binding buffer (pH 7.4; 20 mM imidazole) at a flow rate of 5 mL/min. Subsequently, the protein sample, filtered through a 0.45 μm filter, was loaded onto the column. Unbound proteins were washed away using 5 column volumes of the binding buffer. Unbound proteins were washed out with binding buffer, and *Vm*ChiA was eluted using a buffer containing 400 mM imidazole. Eluted fractions were analyzed using SDS-PAGE (12 %), and fractions containing *Vm*ChiA were pooled. To mitigate the inhibitory effects of phosphate present in the elution buffer, a buffer exchange was

performed using 20 mM citrate buffer (pH 6.0) and a 30 kDa MWCO ultrafiltration device (Amicon® Ultra-15 Merck) at 4 °C. Protein concentration was determined using a PierceTM BCA Protein Assay Kit (Thermo Fisher Scientific).

2.2. Measuring enzyme activity

The dinitrosalicylic acid (DNS) method was used to determine chitinase activity. An enzyme solution (500 μL) was mixed with a substrate solution (20 mM citrate buffer (pH 6.0) containing 2 % colloidal chitin (500 μL)) were incubated at 37 °C for 30 min. DNS reagent (750 μL) was then added and boiled in a water bath for 10 min. The chitinase activity was measured at 540 nm. One unit of chitinase activity was expressed as the amount of enzyme forming 1 μmol N-Acetylglucosamine per minute under the specified conditions [12].

2.3. Biochemical characterization of VmChiA

2.3.1. Effect of pH and temperature on VmChiA activity

The effect of pH on activity was determined at different pH ranging from 2.0 to 11.0. different buffers were used. The enzyme solution was incubated with substrates of different pH values (acetate buffer (pH 2–3), citrate buffer (pH 4–6), Tris-HCl buffer (pH 7–9), sodium carbonate buffer (pH 10–11)) containing 2 % colloial chitin for 30 min at 37 °C and enzyme activity was determined by DNS method. The effect of temperature on activity was determined by measuring the amount of reducing sugar formed after incubating the enzyme solution with the substrate containing 2 % colloidal chitin (20 mM citrate buffer (pH 6) at different temperatures (10 °C–90 °C) for 30 min [12]. To measure the thermal stability of chitinase, the enzyme was incubated at 40 °C for 48 h and the relative activity was determined. pH stability was determined by measuring the relative activity over 48 h in 20 mM citrate buffer (pH 6.0) at 4 °C.

2.3.2. Determination of kinetic parameters of VmChiA

The kinetic parameters of purified *Vm*ChiA (Michaelis Menten constant (K_m) (mM) and maximal velocity (V_{max}) (μmol min^{-1})) were calculated using colloidal chitin as substrate. The effect of substrate concentration on activity was determined by incubating the substrate containing varying concentrations of colloidal chitin with a constant concentration of chitinase at 40 °C for 30 min. Activity was measured in triplicate and kinetic constants were calculated by Lineweaver Burk plot. The turnover number (k_{cat}) (1) and catalytic efficiency (2) were determined using the following Eqs. [38].

$$k_{cat}\ (\mathrm{min}^{-1}) = V_{max}/[E] \quad (1)$$

Where [E] is the enzyme concentration (mg).

$$\text{Catalytic efficiency}\ (\mathrm{mM}^{-1}\ \mathrm{min}^{-1}) = k_{cat}/K_m \quad (2)$$

2.4. Determination of efficacy against A. obtectus

Adult *A. obtectus* individuals were obtained from the Faculty of Agriculture, Atatürk University, Department of Plant Protection. The enzyme was diluted to concentrations 10 U mL^{-1}, 20 U mL^{-1}, 30 U mL^{-1} and 40 U mL^{-1} using a 20 mM citrate buffer (pH 6.0). Four different enzyme doses, water (control) and malathion (200 mL/100 m^2) were sprayed into 250 cm^3 glass jars containing 60 g of beans. The treatment was performed in three replicates for each dose. Then 10 insects were placed in each jar. The jars were labeled and placed in the laboratory (25 ± 1 °C - 60 % ± 5 %). The experiment was carried out in triplicate. Observations were made every 24 h for 7 days and insect mortality was recorded. Corrected mortality rates were calculated using Abbott formula [39].

2.5. Homology modeling, docking and molecular dynamics simulations

2.5.1. Homology modeling

The protein sequence of the *V. maritimus* chitinase (*Vm*ChiA) (UniProtKB: A0A090T850) was retrieved from the UniProt database [36]. The three-dimensional structure of target protein using the SWISS-MODEL application, which employs a known crystal structure as a template [40]. The 3ARR [25] PDB (Protein Data Bank) [41] structure was used as a template to obtain the homology structure of *Vm*ChiA. Here, SWISS-MODEL [40] and the integrated application ProMod3 (Version 3.4.1) [42] were used to predict the 3D homology structure of *Vm*ChiA catalytic domain based on the protein sequence. Global and local model evaluation (GMQE, QMEANDisCo and QMEAN *Z*-score) [43,44] scores and Ramachandran plot analysis [45] were performed to ensure that the homology model obtained was physically possible and acceptable for the protein structure.

2.5.2. Docking

First, the three-dimensional structure of *N*-acetylglucosamine $(GlcNAc)_2$ was drawn and the SMILES code (CC(=O)NC1OC(*CO*)C(O)C(*O*)C1OC1OC(*CO*)C(O)C(*O*)C1NC(C) = O) was defined. Subsequent to obtaining a homology model of *Vm*ChiA and three-dimensional of $(GlcNAc)_2$ ligand structure, the $(GlcNAc)_2$ ligand was docked into the ligand binding domain of *Vm*ChiA structure via the Chimera [46] and Autodock Vina [47,48] applications. Afterwards, PLIP application was used to analyze the protein-ligand interaction profile [49].

2.5.3. Molecular dynamics simulations

CHARMM-GUI application was used to prepare molecular dynamics (MD) simulations scripts [50,51]. In MD simulations, the pH of the system was set to 6.0 and the temperature was set to 313.15 K (40 °C). For the protonation state, ASP57 is labeled with ASPP and GLU61 with GLUP patches. Furthermore, a disulfide bond was set up between the residues Cys155-Cys164. A 10 Å thick rectangular TIP3P water box was used to immerse all structures with K^+ and Cl^- (Neutralized: KCl 0.15 mol L^{-1}). In the system, ions were placed by Monte-Carlo method. CHARMM36m force field was selected. NVT (Canonical) ensemble (temperature 313.15 K, particle numbers 67,762, and volume 729,000 $Å^3$ parameters fixed) was selected for the equilibration phase and NPT (Isothermal-Isobaric) ensemble (temperature 313.15 K, particle numbers 677,759, and pressure 1 atm parameters fixed) was set during the simulation.

The *Vm*ChiA enzyme complex simulation studies were designed as two simulations and named Prot (apoenzyme) and Prot-Lig (holoenzyme, with the $(GlcNAc)_2$). SwissParam application was used to determine the parameters of the $(GlcNAc)_2$ ligand compatible with the CHARMM36m force field. For the *Vm*ChiA simulations, an equilibration and 100 ns MD simulation were performed [52,53]. At first, the system was relaxed through a single-phase energy minimization performed over 10,000 steps. The minimized system was subsequently heated from 0 to 313.15 K during 0.25 ns, applying positional restraints of 1 kcal/(mol $Å^2$) on the protein backbone and ligand. The 100 ns simulation was performed without any restraints. The NAMD application [54,55] was used to perform the MD simulations. The VMD application was used for distance, root mean square deviation (RMSD), root mean square fluctuation (RMSF) calculations, identify the salt bridges and visualization [56].

2.6. Statistical analysis

All statistical analyses were performed using the SPSS 20.0 and Origin Pro 9.1 softwares. Adjusted mortality rates were calculated according to the formula described by Abbott [39]. Lethal concentration (LC_{50} and LC_{90}), lethal time (LT_{50} and LT_{90}) and 95 % confidence intervals were determined by probit analysis. Pest mortality data were analyzed using analysis of variance and differences between means were

determined using the HSD Tukey multiple comparison test. The data obtained were considered statistically significant at $P < 0.05$ and the results were expressed as mean values ± standard deviation (±SD).

3. Results

3.1. Production of VmChiA enzyme

The SDS-PAGE profile of *Vm*ChiA throughout the purification steps is shown in Fig. 1. A distinct protein band corresponding to approximately 60 kDa was observed, indicating the presence of the target enzyme. As detailed in Table 1, the crude cell-free extract initially contained 14.1 mg of total protein with a total activity of 607.0 U, resulting in a specific activity of 43.1 U mg^{-1}. Following Ni^{2+}-NTA affinity chromatography, a substantial reduction in total protein content (to 0.8 mg) was accompanied by a notable increase in specific activity (306.8 U mg^{-1}), corresponding to a 7.1-fold purification and 40.4 % activity yield. Subsequent ultrafiltration further concentrated the enzyme preparation, yielding 0.6 mg of protein with a final specific activity of 320.2 U mg^{-1} and a slight increase in purification fold (7.4), albeit with a reduced overall yield of 31.6 %. These results collectively demonstrate the efficiency of the purification protocol in isolating highly active *Vm*ChiA with minimal contaminating proteins, as also supported by the SDS-PAGE analysis. The amount of purified protein and its retained activity were sufficient for subsequent biochemical and kinetic characterization studies.

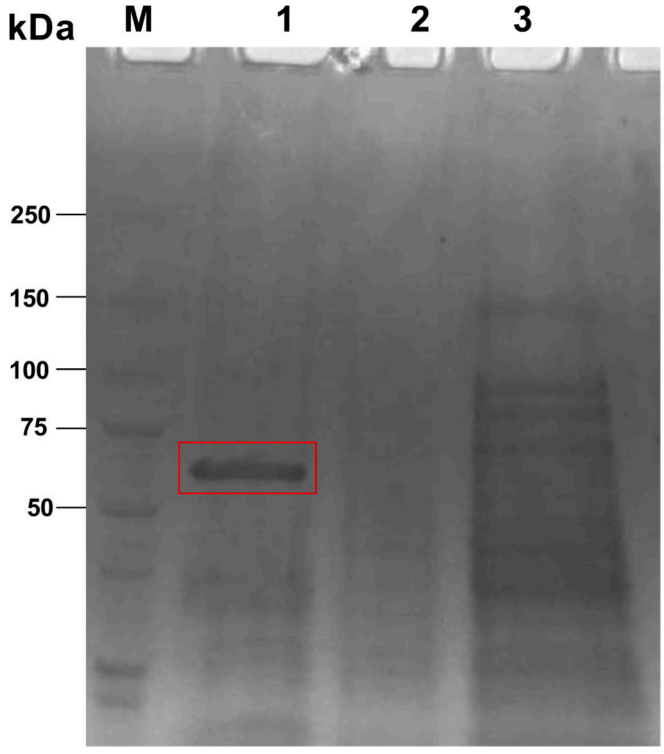


Fig. 1. The SDS-PAGE (12 %) profile of purified *Vm*ChiA. Lane M represents the protein molecular weight marker. Lane 1 shows the purified *Vm*ChiA protein (~60 kDa) eluted from the Ni-NTA affinity column. Lane 2 corresponds to the washing fraction collected after the binding step, indicating the removal of non-specifically bound proteins. Lane 3 represents the flow-through fraction, which contains proteins that did not bind to the Ni-NTA resin during the loading step.

3.2. Biochemical characterization of VmChiA

3.2.1. Optimum pH and temperature of VmChiA

The activity of *Vm*ChiA was measured at different pH conditions and the maximum activity was expressed as 100 % (Fig. 2A). *Vm*ChiA showed its maximum activity against colloidal chitin in citrate buffer at pH 6.0 and retained >75 % of its relative activity at pH 5. Moreover, the enzyme was stable over a wide pH range (pH 3.0–10.0) and the relative activity was close to 40 %. The pH stability of chitinase is shown in Fig. 2B. After incubation in citrate buffer at pH 6.0 for 48 h, chitinase retained 70 % of its activity at 4 h, 63 % at 8 h, 56 % at 24 h and 45 % at 48 h and showed stability at pH 6. The activity of *Vm*ChiA was measured at temperatures ranging from 10 to 90 °C, and the maximum activity was expressed as 100 %. As the reaction temperature increased, the activity of *Vm*ChiA increased and reached a maximum at 40 °C. The enzyme retained >80 % of its relative activity at 50 °C. However, between 60 and 90 °C its relative activity decreased to <40 % (Fig. 2C). Fig. 2D shows the stability of chitinase at 40 °C. Chitinase retained 79 % of its activity at 4 h, 71 % at 8 h, 60 % at 24 h and 48 % at 48 h at 40 °C. These results showed that chitinase was stable at 40 °C.

3.2.2. Kinetic parameters of VmChiA

K_m and V_{max} of the *Vm*ChiA were determined as 0.042 mM and 17.48 μmol min^{-1} by using the Lineweaver-Burk Plot (Fig. 3). The k_{cat} and catalytic efficiency of the enzyme were determined as 1.75 min^{-1}, 41.61 mM^{-1} min^{-1} respectively.

3.3. Efficacy of VmChiA against A. obtectus

When the efficacy of recombinant *Vm*ChiA was tested against *A. obtectus*, it was observed that the impact on mortality was highly significant ($F = 55.3$, $df = 5$, $p = 0.00$). Mortality rates varied significantly, ranging from 33.3 % to 100 % ($P < 0.05$) by the end of the 10th day (Table 2). The highest efficacy was observed with the commercial insecticide malathion and the 40 U mL^{-1} *Vm*ChiA dose, both resulting in 100 % mortality, followed by 30 U mL^{-1} with 96.7 % mortality. While the difference between these three treatments was statistically insignificant ($P > 0.05$), the difference between them and 10 U mL^{-1}, 20 U mL^{-1} and control was significant ($P < 0.05$). The dose of 20 U mL^{-1} reached a mortality rate of 60 % and the lowest *Vm*ChiA dose of 10 U mL^{-1} reached a mortality rate of 33.3 % compared to the control at the end of day 10. The difference between the two doses and the control was significant ($P < 0.05$). Probit analysis (Finney's method) was used to estimate the lethal doses and durations that caused 50 % and 90 % of the population to die. The probit mortality regression data (LC_{50} and LC_{90}) are presented in Table 3 along with other estimated probit parameters. The lethal concentrations (LC_{50} and LC_{90}) of *Vm*ChiA against *A. obtectus* were 13.95 U mL^{-1} (11.29–16.28) and 27.66 U mL^{-1} (23.13–36.87), respectively (Table 3). Moreover, the dose-dependent lethal times (LT_{50} and LT_{90}) were 3.4 d (2.9–3.8) and 7.5 d (6.6–9.1) for 40 U mL^{-1}, 4.6 d (4.0–5.2) and 11.3 d (9.4–15.2) for 30 U mL^{-1}, and 8.4 d (7.0–10.8) for 20 U mL^{-1}, respectively (Table 4). Since 90 % mortality rate could not be reached at 20 U mL^{-1}, LT_{90} value was not determined, and since both mortality rates (50 % and 90 %) could not be reached at 10 U mL^{-1}, LT_{50} and LT_{90} values were not determined.

3.4. In silico analysis

The homology modeling results of the *Vm*ChiA catalytic domain (Fig. 4) showed a GMQE score of 0.55, a QMEANDisCo Global value of 0.90 ± 0.05, and a sequence identity of 82.40 %. The QMEAN value was calculated as 1.58, and Ramachandran analysis revealed that 97 % of the residues were located in favored regions, with 100 % in allowed regions and no outliers (Fig. S1). During MD simulations, RMSD values ranged between 2 and 3.5 Å for the Prot simulation, while the Prot-Lig simulation exhibited a more stable structure with fluctuations around 2 Å.

Table 1
*Vm*ChiA purification process.

Purification steps	Volume (mL)	Total Protein (mg)	Total Activity (U)	Specific Activity (U mg^{-1})	Purification (Fold)	Activity Yield (%)
Cell free extract	10.0	14.1	607.0	43.1	1.0	100
Ni^{2+}-NTA purification	4.8	0.8	245.4	306.8	7.1	40.4
Ultrafiltration	2.4	0.6	192.1	320.2	7.4	31.6

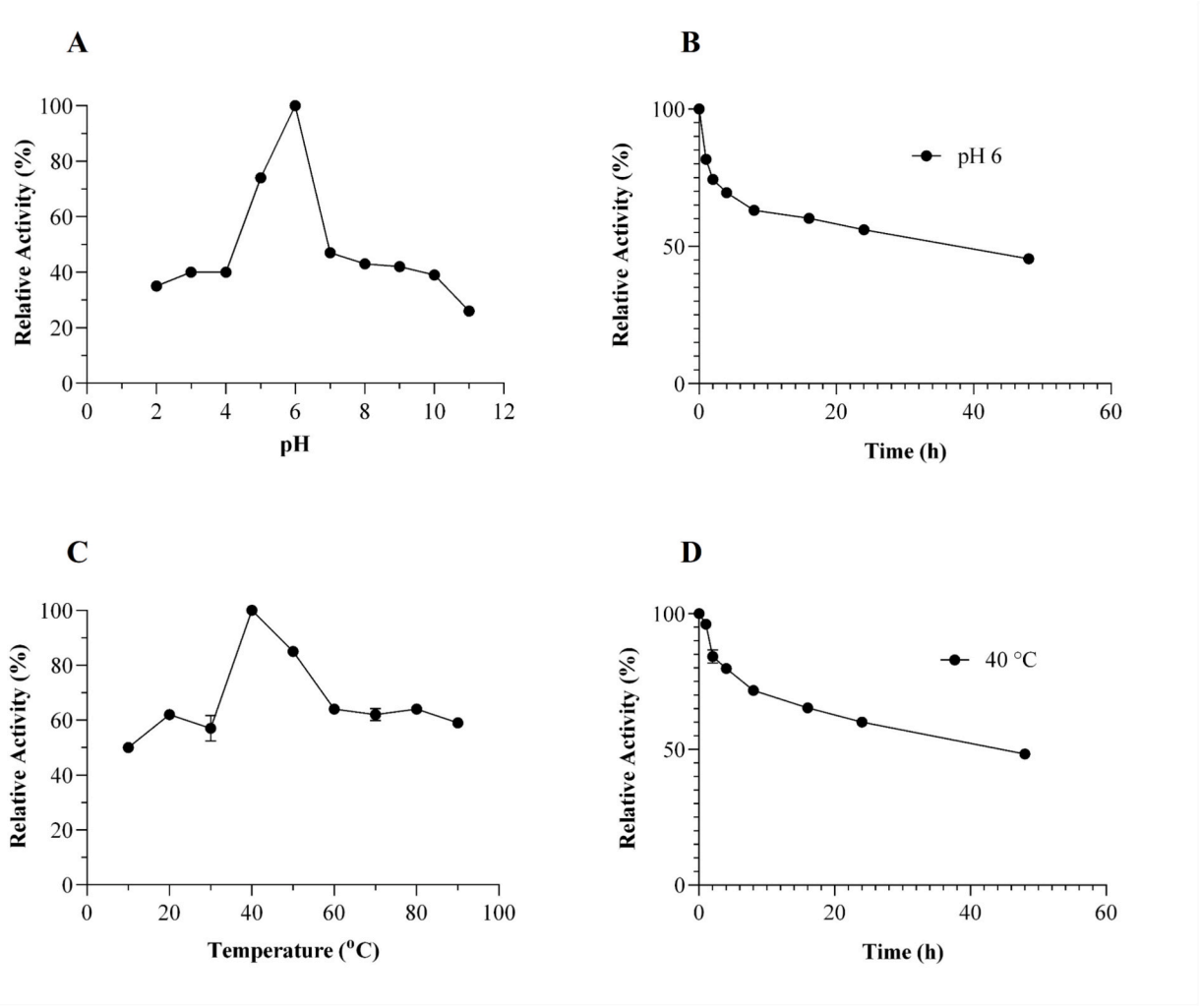


Fig. 2. Effect of pH (**A, B**) and temperature (**C, D**) on the activity and stability of recombinant *Vm*ChiA.

The average RMSD values were 2.69 Å and 2.27 Å for Prot and Prot-Lig simulations, respectively (Fig. S2). RMSF analysis indicated local mobility in Gly67 and neighboring amino acids for the Prot-Lig simulation after the ligand $(GlcNAc)_2$ exited the binding pocket, whereas Asp172 and neighboring residues showed significant motion in the Prot simulation (Fig. S3). Salt bridge analysis revealed that the Glu274-Arg296 salt bridge remained intact in the Prot simulation but was disrupted after ~10 ns in the Prot-Lig simulation, suggesting structural rearrangement (Fig. 5–6). Key interactions between Trp21 and Trp143 residues of *Vm*ChiA and the $(GlcNAc)_2$ ligand were observed as the ligand exited the binding pocket.

4. Discussion

Vibrio species, commonly found in oceans and seas, are natural chitin degraders and often produce large amounts of chitinolytic enzymes to hydrolyze hard chitin [57,58]. Therefore, in the present study, the chitinase gene of a chitinolytic strain V. maritimus was expressed in E. coli and purified. Some biochemical properties of purified VmChiA and its activity against A. obtectus, an important agricultural pest, were tested. The recombinant VmChiA (320.2 U mg^{-1}) exhibited a higher specific activity than many chitinases available in the literature, such as Chi4733 (175.5 U mg^{-1}), Chi540 (134.5 U mg^{-1}) Chi4668 (39.5 U mg^{-1}), VhChit2 (36.5 U mg^{-1}), SaChiB (28.4 U mg^{-1}), VhChit6 (20.8 U mg^{-1}), rCHI-2 (19.0 U mg^{-1}), Ce0303 (6.41 U mg^{-1}), MaChi1 (1.78 U mg^{-1}) and CaChiT (0.2 U mg^{-1}) [58–63]. The molecular mass of VmChiA was determined to be ~60 kDa and was similar to Vibrio chitinases such as VhChit6 (60 kDa), Chi4668 (61.15 kDa), Chi1557 (61 kDa), Chi2497 (62.24 kDa) and VhChiA (63 kDa) [57,58,62,64].

To date, most of the chitinases available in the literature have been reported to show optimum activity at an acidic or near-neutral pH and generally in the range of 40–60 °C [10,65,66]. However, the optimum pH and temperature of chitinases often vary even within the same species. For most *Vibrio*-derived chitinases, the optimum temperature has

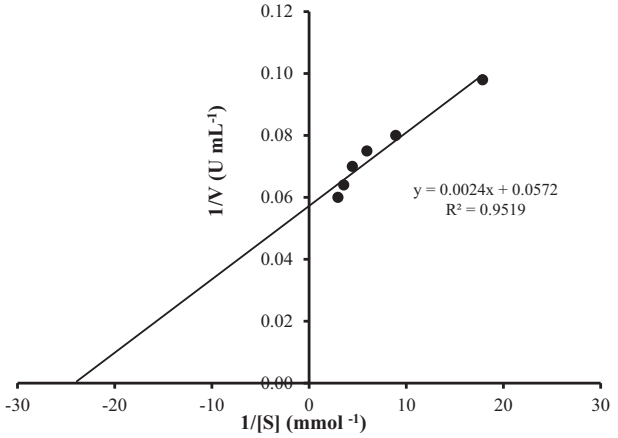


Fig. 3. Lineweaver-Burk plot of *Vm*ChiA versus collodial chitin concentration.

Table 2
Insecticidal activity of recombinant *Vm*ChiA against *A. obtectus* adults.

Chitinase Dose (U mL^{-1})	Mortality Rate (%) ± SD*
Water (Control)	0.0 ± 0.0[d]
10	33.3 ± 15.3[c]
20	60.0 ± 17.3[b]
30	96.7 ± 5.8[a]
40	100.0 ± 0.0[a]
Malathion	100.0 ± 0.0[a]

* Letters indicate differences between groups (Tukey's HSD test, $P < 0.05$), SD: Standard deviation.

Table 3
Lethal concentrations (LC_{50} and LC_{90}) of *Vm*ChiA against *A. obtectus* after 10 days of exposure.

	LC_{50} (U mL^{-1}) (95 % CL)	LC_{90} (U mL^{-1}) (95 % CL)	χ^2	df	*p* value
VmChiA	13.95 (11.29–16.28)	27.66 (23.13–36.87)	5.80	2	0.055

LC_{50}: The concentration that causes the death of 50 % of insects after treatment, LC_{90}: The concentration that causes the death of 90 % of insects after treatment, CL: confidence limits, χ^2: Chi-square, df: degrees of freedom.

Table 4
Effect of *Vm*ChiA doses on the lifespan of *A. obtectus* adults.

*Vm*ChiA Dose (U mL^{-1})	LT_{50} (d) (95 % CL)	LT_{90} (d) (95 % CL)	χ^2	df	p value
10	ND*	ND*	–	–	–
20	8.4 (7.0–10.8)	ND*	1.25	8	0.996
30	4.6 (4.0–5.2)	11.3 (9.4–15.2)	10.63	7	0.156
40	3.4 (2.9–3.8)	7.543 (6.6–9.1)	9.35	8	0.313

* ND (not determined) indicates that values could not be calculated because mortality was <50 % or 90 %, LT_{50}: 50 % of insects dead after treatment, LT_{90}: 90 % of insects dead after treatment, CL: confidence limits, χ^2: Chi-square, df: degrees of freedom.

been reported to be 45–55 °C and the optimum pH in the range of 6.0–8.0 [64]. The purified *Vm*ChiA exhibited a similar optimal pH profile as *Vibrio* sp. 98CJ11027 [67], *V. rotiferianus* [64], *V. harveyi* [64] and *V. harveyi* WXL538 [62] chitinases, reaching maximum activity in slightly acidic conditions (pH 6.0). The optimum temperature (40 °C) of the recombinant *Vm*ChiA was lower than that of previously described *Vibrio* chitinases (Chi1557 (45–50 °C) Chi4668 (~50 °C), *Vh*Chit2 (50 °C) and *Vh*Chit6 (50 °C), while it was in agreement with *Streptomyces mutabilis* IMA8, *S. griseoinacarnatus* RB7AG, *Aeromonas* sp. CQNU6–2,

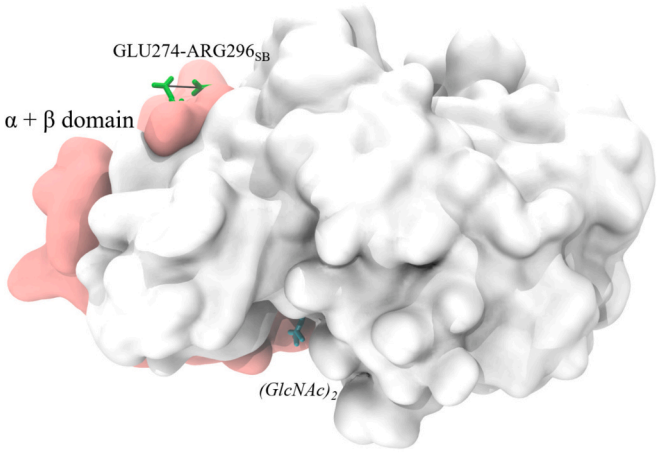


Fig. 4. Structure of the catalytic domain of *Vm*ChiA. Salt bridge-associated residues (GLU274-$ARG296_{SB}$) in the α + β domain (pink) is shown in green. The ligand $(GlcNAc)_2$ is shown in cyan.

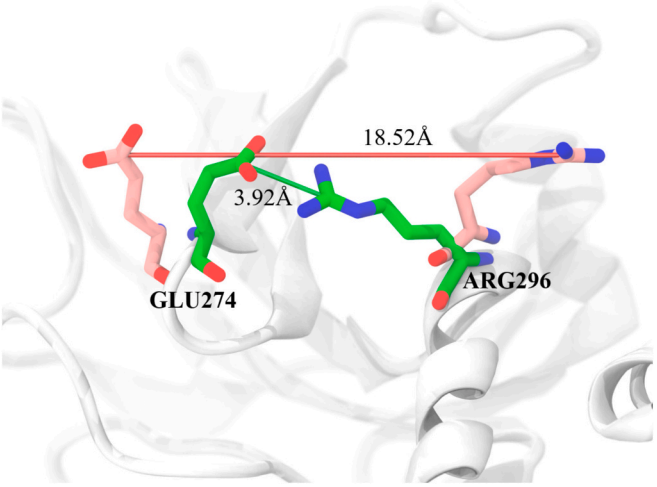


Fig. 5. A frame from the Prot-Lig simulation showing the longest distance of the disengaged salt bridge between residues Glu274 and Arg296 at 82 ns (18.52 Å). The green licorine and line represent Prot, the pink licorine and line represent Prot-Lig simulations. The red licorine points represent oxygen atoms and the blue ones represent nitrogen atoms.

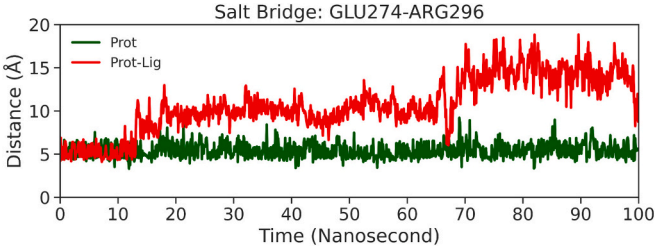


Fig. 6. Plot of the distance change of the salt bridge between residues GLU274 and ARG296 during 100 ns.

Chitinibacter tainanensis CT01 ve *Bacillus cereus* NK91 [58,62,64,68–72]. The kinetic parameters of chitinase against different substrates have been evaluated in the literature [73,74]. In the present study, colloidal chitin was used as substrate and various studies are given in Table 5 as an example. The low K_m value (0.042 mM) exhibited by *Vm*ChiA

Table 5
Some biochemical and kinetic properties of chitinases isolated from different sources.

Enzyme source	Used substrate	Optimum conditions		Kinetic parameters		Molecular weight (kDa)	Specific activity (U mg^{-1})	**Reference**
		pH	°C	K_m	V_{max}			
Vibrio maritimus	Colloidal chitin	6	40	0.042 mM	17.48 μmol min^{-1}	60	320.2	This study
Streptomces chilikensis	Colloidal chitin	7	60	0,02 mM	3184 mol min^{-1}	10,5	60.53	[75]
Paenibacillus sp.	Colloidal chitin	4.5	50	4.28 mg mL^{-1}	14.29 μg min^{-1} mL^{-1}	30	0.85	[76]
Penicillium oxalicum k10	Colloidal chitin	5.5	40	12.56 mg mL^{-1}	1.05 μM min^{-1} mg^{-1}	45	162.1	[77]
Thermomyces lanuginosus	Colloidal chitin	6.5	50	212.3 μM	352.8 μmol min^{-1}	18	88.64	[78]
Bacillus cereus	Colloidal chitin	7,0	40	0,07 mg mL^{-1}	76,9 μmol min^{-1}	43.7	8.52	[79]
Stenotrophomonas maltophilia	Colloidal chitin	7.0	50	1.6419 mg mL^{-1}	16.129 U mg^{-1}	52	5.81	[80]
Aeromonas media CZW001	Colloidal chitin	8.0	55	5.26 mg mL^{-1}	6.9 U mg^{-1}	40	10.37	[81]
Chaetomium globosum W7	Colloidal chitin	5.0	45	3.18 mg ml^{-1}	8.05 μmol min^{-1} mg^{-1}	60	5.21	[82]
Chitinilyticum aquatile CSC-1	Colloidal chitin	6.0	45	1.159 mg mL^{-1}	10.37 μM min^{-1} $mg-^{1}$	47	3.48	[83]

towards colloidal chitin reflects the high affinity of the enzyme for its substrate. Furthermore, kinetic analyses performed under optimum conditions indicate that *Vm*ChiA has a good potential for the biodegradation of chitin. Suryawanshi and Eswari [78] determined K_m and V_{max} values as 212.3 μM and 352.8 μmol min^{-1}, respectively. Thakur et al. [79] found K_m and V_{max} values as 0.07 mg mL^{-1} and 76.9 μmol min^{-1}, respectively, and Du et al. [76] found them as 4.28 mg mL^{-1} and 14.29 μg min^{-1} mL^{-1}.

Chitinase enzymes are widely used in various industries such as medicine (anti-inflammatory drugs, ulcerative colitis, anticancer and anti-tumour, contact lenses, artificial skin and surgical sutures, etc.) [84,85], food (improving fruit and vegetable processing processes and fermentation conditions) [86], cosmetics (skin renewal products and hair care applications) [87] and biotechnology (genetic engineering applications and protein production) [88]. The versatile industrial applications of this enzyme have great potential for the development of sustainable production processes. Recombinant *Vm*ChiA exhibited better biochemical properties compared to many microbial-derived chitinases available in the literature considering its thermal stability, pH stability and specific activity [76,80,89].

The idea of using chitinases as bioagents in agricultural production stems from the fact that chitin is a structural component in the exoskeleton, trachea and peritrophic matrix of insects and is absent in higher organisms. Moreover, the special potential of chitinases for pest inhibition without disrupting the ecosystem has made them a safe and effective strategy for the development of new pesticides [16]. The insecticidal activity of VmChiA was evaluated against A. obtectus, the major pest of stored beans. The recombinant enzyme resulted in 100 % mortality in A. obtectus adults, with mortality increasing in parallel as the dose of chitinase increased. When the 40 U mL^{-1} dose of VmChiA was compared with the commonly used chemical insecticide (malathion), there was no difference in mortality, with both treatments reaching 100 % mortality. Malathion reached 100 % mortality within a few hours after treatment, while VmChiA (40 U mL^{-1}) reached 99 % mortality in a longer period of 7 days. Although malathion shows the desired effect in a much shorter time, considering its negative effects [90,91], VmChiA, which has a longer duration of efficacy, can be a good alternative to chemical insecticides because it is environmentally friendly and has no toxic effects on humans.

The lethal effect of VmChiA on insects is likely to result from damage to the peritrophic membrane lining the midgut epithelium and the cuticle through contact after feeding on the chitinase-treated diet. Indeed, this has been proven by histological observations made in previous studies [80,92,93]. Numerous studies have also highlighted the efficacy of chitinase and chitinase-producing microorganisms against agricultural pests [15,94]. For example, ChiA-Si40 was tested against adults and larvae of Sitophilus granarius and a dose of 25 μg mL^{-1} was reported to cause 100 % mortality after 1 h of exposure [92]. Chitinase immobilized on ZnO nanoparticle was tested against S. zeamais and 6 mg L^{-1} caused 100 % mortality in insects [12]. Similarly, the chitinase ChiB was evaluated against Spodoptera frugiperda and high mortality rates, impaired development and reduced larval population were observed [16]. In addition, as a result of the 5-day treatment of Leptinotarsa decemlineata with chitinase, it was determined that the heads and legs of the insects were detached and the tight structure of the hexagonal cells on the elytra surface was disrupted [80]. Again, oral administration of Trichoderma asperellum chitinase to Bombyx mori larvae negatively affected their survival and development [93]. In addition, Tawfiq et al. [95] tested the insecticidal activity of chitinase immobilized on cobalt metal-organic framework on T. castaneum and reported that the mortality rate at the end of the fourth day was 100 % for immobilized chitinase and 25 % for free chitinase. When the results obtained were compared with the literature results, it was determined that similar insecticidal effects were observed even if the source of chitinase and the insects treated were changed. These findings highlight chitinases isolated from different microbial sources in the biological control of pests and emphasize the utility of chitinases as an effective strategy in agricultural production to reduce the use of hazardous pesticides.

VmChiA can be integrated into broader biocontrol strategies by combining it with other bioactive agents or microbial consortia targeting multiple pest species. Chitinases have shown synergistic effects when used in combination with entomopathogenic fungi, B. thuringiensis toxins or other microbial pesticides, increasing overall pest suppression [93,96,97]. In addition, its use in combination with other control methods can reduce the development of resistance in insects.

*Vm*ChiA catalytic domain homology modeling results based on the 3ARR [25], template are shown in Table 6. The GMQE (Global Model Quality Estimate) value estimates the overall quality of the model and assumes a value between 0 and 1 [98]. A GMQE score of 0.55 was obtained during modeling. QMEANDisCo Global value of 0.90 ± 0.05 mentioned that the overall quality of the model is high [44]. A sequence identity of 82.40 % indicated that the model is based on a correct template structure and is generally reliable. In homology modeling, a

Table 6
*Vm*ChiA catalytic domain homology modeling results based on the 3ARR template.

Template	Seq identity	Oligo state	Seq Similarity	GMQE Score	QMEANDisCo Score ± SD*
3ARR	82.40 %	monomer	0.58	0.55	0.90 ± 0.05

* SD: Standard deviation.

sequence identity above 30 % generally provides acceptable model quality [99,100]. The QMEAN value of 1.58 indicates that the overall quality of the model is above average (QMEAN *Z*-Scores: 1.58, Cβ (C-beta): 1.53, All Atom: −0.70, Solvation: −0.35, and Torsion: 1.49) [101]. The Ramachandran plot analysis showed that 97 % of the residues in the model are located in the favored regions and 100 % in the allowed region in Fig. S1. In addition, no outliers were observed in the Ramachandran plot analysis [45]. The structure of the *Vm*ChiA catalytic domain obtained from the Swiss-Model application [40] has a very high structural quality. Especially the results of QMEAN and Ramachandran analysis showed that the overall structural integrity of the model is strong.

The MD simulations were designed as two simulations, named Prot and Prot-Lig, with the pH of the system set to 6.0 and the temperature set to 313.15 K (40 °C). It has been previously reported that temperature and pH values are suitable conditions to initiate MD simulations. Moreover, it has been demonstrated that the TIM-barrel structure is retained at these conditions [32]. The structure of the catalytic domain of *Vm*ChiA was modeled with the Swiss-Model application [40] and visualized with the VMD application [56] and is shown in Fig. 4. RMSD analysis was performed to evaluate how much the *Vm*ChiA catalytic domain deviates from the initial reference structure (0 ns) and to evaluate the stability during the simulations. RMSD values for protein Cα atoms were observed during 100 ns simulations. Prot (Green) typically fluctuated in the range of 2–3.5 Å throughout the simulation (Fig. S2). Moreover, Prot-Lig (Red) showed a more stable structure and was frequently observed to fluctuate around 2 Å. Prot-Lig simulation can be considered to have a more stable structure with lower RMSD values than Prot simulation. Similarly, in previous studies, the RMSD of *Ov*CHT1 was observed to be around 2 Å during 10 ns of simulation [29]. In the present study, the average RMSD values of protein Cα atoms were observed 2.69 Å and 2.27 Å for Prot and Prot-Lig simulations, respectively (Fig. S2). In the Prot-Lig simulation, after the ligand exits the binding pocket at 50.ns, the RMSD is lower than in the Prot simulation, suggesting that the main structure of the protein remains stable and that the exit of the ligand unlead to a major change in the global structure of the protein.

Additionally, in the time range 0–100 ns, RMSF analysis was performed to study the average positional deviation of *Vm*ChiA catalytic domain atoms and protein dynamics. The RMSF values were analyzed in two different ways: for the first 50 ns (Fig. S3A), meaning until the moment when the ligand $(GlcNAc)_2$ exits the binding pocket in the Prot-Lig simulation, and for the RMSF values of the all simulations (Fig. S3B). A significant peak was observed in the first 50 ns and 100 ns, especially at residue Gly67 and neighboring amino acids for the Prot-Lig simulation. However, for the Prot 100 ns simulation, only residue Asp172 and neighboring amino acids showed a significant peak. The local movements of Gly67 residue and neighboring amino acids, the amino acids in the binding pocket of the $(GlcNAc)_2$ ligand were observed. However, the motion of Asp172 residue was noticed as a loop movement and this region was observed to approach the α + β domain. Nevertheless, this motion was unobserved in the Prot-Lig simulation. Furthermore, salt bridges in the *Vm*ChiA catalytic domain were investigated to correlate the structural changes observed in the RMSD and RMSF analyses.

The Salt Bridges plugin of the VMD application [56] was utilized to define salt bridges in the structure by searching for ion pairs with an oxygen-nitrogen distance within 3.2 A and measuring their distances. In 100 ns simulations, 36 salt bridges were detected for the Prot simulation and 39 for the Prot-Lig simulation. In particular, the distance of the salt bridge between Glu274 and Arg296 in the α + β domain of VmChiA structure was significantly different between the two simulations (Fig. 5). The GLu274-Arg296 salt bridge was intact in the Prot simulation, whereas in the Prot-Lig simulation, the bridge was observed to be no longer intact after ~10 ns (Fig. 6). The dramatic decreases in the distance of the Glu274-Arg296 salt bridge in the Prot-Lig simulation, especially after the ligand exits from the binding pocket, suggests that the protein is in a process of structural rearrangement to recover the distance of the Glu274-Arg296 salt bridge (Fig. 6).

Many studies have reported key amino acids in the binding pocket of the family 18 chitinases [20,23,25,27]. For instance, Trp275 and Trp397 residues of VhChiA structure (PDB: 3ARR) were reported to be important for the binding of inhibitors in terms of hydrophobic interactions [25]. Likewise, the role of Trp residues in the structure of chitinase B has also been determined [102]. However, the major difference between ChiA and ChiB is considered to be the structure of the loops that form a 'roof' over the active zone [23]. In the current study, the interaction between VmChiA and (GlcNAc)2 ligand was analyzed by PLIP application [49] with frames every ten nanoseconds until the ligand exits the binding pocket (Table 7). When the VmChiA structure was superimposed with the other ChiA (PDB: 1CTN) structure [103], Trp275 corresponds to Trp21 in VmChiA. Moreover, when it compared to a ChiB (PDB: 1E15) structure [102], residue Trp220 overlaps with Trp143. In addition, in the ChiA (PDB: 3ARR) structure [25], the template the catalytic domain of the VmChiA structure, Trp397 superimposed Trp143 in VmChiA. Table 7 shows the interactions of the VmChiA structure with Trp21 and Trp143 as the ligand $(GlcNAc)_2$ exits the ligand binding pocket.

5. Conclusions

The chitinase gene of *V. maritimus* was successfully cloned and expressed in *E. coli* BL21. *Vm*ChiA, which was found to be mesophilic (40 °C) and acidic (pH 6.0), exhibited good insecticidal activity against *A. obtectus*, indicating that it could be a potential biocontrol candidate for reducing crop losses due to insect pests in sustainable agriculture. To enhance the long-term applicability of *Vm*ChiA in agricultural settings, its stability can be improved by various biotechnological strategies. Immobilization of *Vm*ChiA on biocompatible supports (e.g., chitosan beads, silica matrices) or encapsulation in biodegradable polymers (e.g., alginate, polyvinyl alcohol) can provide protection against environmental stressors and thus extend its functional life in storage applications. Further studies and observations are needed to better understand the inhibition mechanism of chitinase on pests and to reveal its efficacy on different pests. The Prot-Lig simulation showed that the protein was in the process of a structural rearrangement to restore the distance of the Glu274-Arg296 salt bridge. However, this rearrangement was hardly occurred. This process was suggested to contribute to the α + β domain of *Vm*ChiA providing an open, deep active binding cleft around the substrate binding site of the enzymes. Further structural studies are needed to clarify the role of the Glu274-Arg296 salt bridge in the 'slide and bend' mechanism.

Table 7
Time-dependent variation of hydrophobic interactions and hydrogen bonds while the $(GlcNAc)_2$ exits the binding pocket.

Time	Hydrophobic Interactions	Hydrogen Bonds
0 ns*	ASP 138	TRP 21, TYR 62, GLN 66, LYS 116
10 ns	TRP 143, ASP 245	ASP 138, ARG 209, GLU 244
20 ns	TRP 143	LYS 116, ASP 138, GLY 142, ARG 209
30 ns	ASP 138, TRP 143, ASP 245	GLY 142, ARG 209, ASP 245
40 ns	TYR 140	ASP 115, ASN 144, LYS 177, TYR 181

* First frame after equilibration process.

CRediT authorship contribution statement

Neslihan Dikbaş: Writing – review & editing, Writing – original draft, Supervision, Methodology, Conceptualization. **Ahmet Tülek:** Writing – review & editing, Methodology, Investigation, Conceptualization. **Sevda Uçar:** Writing – original draft, Visualization, Investigation, Data curation. **Şeyma Alım:** Writing – original draft, Visualization, Investigation, Data curation. **Burak Servili:** Writing – review & editing, Visualization, Investigation. **Nurettin Paçal:** Visualization, Investigation. **Göksel Tozlu:** Writing – review & editing, Investigation. **Sezai Ercisli:** Writing – review & editing.

Funding

The authors declare that no funds, grants, or other support were received during the preparation of this manuscript.

Declaration of competing interest

The authors have no relevant financial or non-financial interests to disclose.

Appendix A. Supplementary data

Supplementary data to this article can be found online at https://doi.org/10.1016/j.ijbiomac.2025.144285.

Data availability

All data are presented in the article.

References

[1] M. Díaz-Díaz, A. Bernal-Cabrera, A. Trapero, A.J. González, R. Medina-Marrero, R.D. Cupull-Santana, E. Águila-Jiménez, C. Agustí-Brisach, Biocontrol of root rot complex disease of *Phaseolus vulgaris* by *Streptomyces* sp. strains in the field, Crop Prot. 165 (2023) 106164, https://doi.org/10.1016/j.cropro.2022.106164.

[2] T.B. Wekesa, V.W. Wekesa, J.M. Onguso, E.N. Wafula, N. Kavesu, Isolation and characterization of *Bacillus velezensis* from lake Bogoria as a potential biocontrol of *fusarium solani* in *Phaseolus vulgaris* L, Bacteria 1 (2022) 279–293, https://doi.org/10.3390/bacteria1040021.

[3] J. Lazarević, S. Jevremović, I. Kostić, M. Kostić, A. Vuleta, S. Manitašević Jovanović, D. Šešlija Jovanović, Toxic oviposition deterrent and oxidative stress effects of *Thymus vulgaris* essential oil against *Acanthoscelides obtectus*, Insects 11 (2020) 563, https://doi.org/10.3390/insects11090563.

[4] J. Vuts, S.J. Powers, E. Venter, Á. Szentesi, A semiochemical view of the ecology of the seed beetle *Acanthoscelides obtectus* say (Coleoptera: Chrysomelidae, Bruchinae), Ann. Appl. Biol. 184 (2024) 19–36, https://doi.org/10.1111/aab.12862.

[5] J. Lazarević, S. Jevremović, I. Kostić, A. Vuleta, S. Manitašević Jovanović, M. Kostić, D. Šešlija Jovanović, Assessment of sex-specific toxicity and physiological responses to thymol in a common bean pest *Acanthoscelides obtectus* say, Front. Physiol. 13 (2022) 842314, https://doi.org/10.3389/fphys.2022.842314.

[6] M. Chinji, S. Hamabwe, K. Kuwabo, I. Mugovu, R. Thole, M. Mazala, J.M. Osorno, P. McClean, C. Jochua, C. Urrea, C. Mukuma, V. Chisale, K. Kamfwa, Introgression and stability of common bean weevil (*Acanthoscelides obtectus* [say]) resistance in diverse market classes from the andean gene pool of common bean, Legum. Sci. 6 (2024) e223, https://doi.org/10.1002/leg3.223.

[7] Á. Rodríguez-González, P.A. Casquero, V. Suárez-Villanueva, G. Carro-Huerga, S. Álvarez-García, S. Mayo-Prieto, A. Lorenzana, R.E. Cardoza, S. Gutiérrez, Effect of trichodiene production by *Trichoderma harzianum* on *Acanthoscelides obtectus*, J. Stored Prod. Res. 77 (2018) 231–239, https://doi.org/10.1016/j.jspr.2018.05.001.

[8] A.S. Abdel-Baki, M. Samar, S.M. Ibrahium, A.O. Aboelhadid, S.A. Hassan, H. Abdel-Tawab, Benzyl alcohol, benzyl benzoate and methyl benzoate as bio-insecticides against dried bean beetle *Acanthoscelides obtectus* (Coleoptera: Tenebrionidae), J. Stored Prod. Res. 105 (2024) 102246, https://doi.org/10.1016/j.jspr.2024.102246.

[9] İ. Rat, M. Mamay, Demographic parameters of *Anthocoris minki* Dohrn (Hemiptera: Anthocoridae) reared on common bean (*Phaseolus vulgaris* L.), faba bean (*Vicia faba* L.) and pea (*Pisum sativum* L.) as egg laying media, Neotrop. Entomol. 53 (2024) 531–540, https://doi.org/10.1007/s13744-024-01133-w.

[10] R. Liu, J. Li, F. Zhang, D. Zheng, Y. Chang, L. Xu, L. Huang, Biocontrol activity of *Bacillus velezensis* D4 against apple Valsa canker, Biol. Control 163 (2021) 104760, https://doi.org/10.1016/j.biocontrol.2021.104760.

[11] A. Ezzine, S. Ben Hadj Mohamed, S. Bezzine, Y. Aoudi, M.R. Hajlaoui, L. Baciou, I. Smaali, Improved expression of a thermostable GH18 bacterial chitinase in two different *Escherichia coli* strains and its potential use in plant protection and biocontrol of phytopathogenic fungi, Mol. Biotechnol. 66 (9) (2024) 1–13, https://doi.org/10.1007/s12033-023-01041-1.

[12] N. Dikbaş, S. Uçar, G. Tozlu, T.Ö. Özer, R. Kotan, Bacterial chitinase biochemical properties, immobilization on zinc oxide (ZnO) nanoparticle and its effect on *Sitophilus zeamais* as a potential insecticide, World J. Microbiol. Biotechnol. 37 (2021) 1–14, https://doi.org/10.1007/s11274-021-03138-8.

[13] A. Beygmoradi, A. Homaei, R. Hemmati, P. Santos-Moriano, D. Hormigo, J. Fernández-Lucas, Marine chitinolytic enzymes, a biotechnological treasure hidden in the ocean? Appl. Microbiol. Biotechnol. 102 (2018) 9937–9948, https://doi.org/10.1007/s00253-018-9385-7.

[14] S. Mahmood, M. Kumar, P. Kumari, G.K. Mahapatro, N. Banerjee, N.B. Sarin, Novel insecticidal chitinase from the insect pathogen *Xenorhabdus nematophila*, Int. J. Biol. Macromol. 159 (2020) 394–401, https://doi.org/10.1016/j.ijbiomac.2020.05.078.

[15] N. Dikbaş, S. Ucar, G. Tozlu, T.Ö. Özer, R. Kotan, The effect of immobilized chitinase enzyme on the biocontrol of Sitophilus zeamais, Turk. J. Agric. For. 47 (2023) 170–177, https://doi.org/10.55730/1300-011X.3075.

[16] G.M. El-Sayed, M.T. Emam, M.A. Hammad, S.H. Mahmoud, Gene cloning, heterologous expression, and in silico analysis of chitinase B from *Serratia marcescens* for biocontrol of *Spodoptera frugiperda* larvae infesting maize crops, Molecules 29 (2024) 1466, https://doi.org/10.3390/molecules29071466.

[17] N. Dahiya, R. Tewari, G.S. Hoondal, Biotechnological aspects of chitinolytic enzymes: a review, Appl. Microbiol. Biotechnol. 71 (2006) 773–782, https://doi.org/10.1007/s00253-005-0183-7.

[18] V. Lombard, H. Golaconda Ramulu, E. Drula, P.M. Coutinho, B. Henrissat, The carbohydrate-active enzymes database (CAZy) in 2013, Nucleic Acids Res. 42 (2014) D490–D495, https://doi.org/10.1093/nar/gkt1178.

[19] A. Beygmoradi, A. Homaei, R. Hemmati, J. Del Arco, J. Fernández-Lucas, Identification of a novel tailor-made chitinase from white shrimp Fenneropenaeus merguiensis, Colloids Surf. B: Biointerfaces 203 (2021) 111747, https://doi.org/10.1016/j.colsurfb.2021.111747.

[20] W. Chen, X. Jiang, Q. Yang, Glycoside hydrolase family 18 chitinases: the known and the unknown, Biotechnol. Adv. 43 (2020) 107553, https://doi.org/10.1016/j.biotechadv.2020.107553.

[21] T. Watanabe, K. Kobori, K. Miyashita, T. Fujii, H. Sakai, M. Uchida, H. Tanaka, Identification of glutamic acid 204 and aspartic acid 200 in chitinase A1 of *Bacillus circulans* WL-12 as essential residues for chitinase activity, J. Biol. Chem. 268 (1993) 18567–18572.

[22] H. Li, L.H. Greene, Sequence and structural analysis of the chitinase insertion domain reveals two conserved motifs involved in chitin-binding, PLoS One 5 (2010) e8654, https://doi.org/10.1371/journal.pone.0008654.

[23] M. Sørlie, H. Zakariassen, A.L. Norberg, V.G.H. Eijsink, Processivity and substrate-binding in family 18 chitinases, Biocatal. Biotransformation 30 (2012) 353–365, https://doi.org/10.3109/10242422.2012.676282.

[24] X. Sun, Y. Li, Z. Tian, Y. Qian, H. Zhang, L. Wang, A novel thermostable chitinolytic machinery of *Streptomyces* sp. F-3 consisting of chitinases with different action modes, Biotechnol. Biofuels 12 (2019) 1–12, https://doi.org/10.1186/s13068-019-1472-1.

[25] S. Pantoom, I.R. Vetter, H. Prinz, W. Suginta, Potent family-18 chitinase inhibitors: x-ray structures, affinities, and binding mechanisms, J. Biol. Chem. 286 (2011) 24312–24323, https://doi.org/10.1074/jbc.M110.183376.

[26] W. Suginta, P. Sirimontree, N. Sritho, T. Ohnuma, T. Fukamizo, The chitin-binding domain of a GH-18 chitinase from *Vibrio harveyi* is crucial for chitin-chitinase interactions, Int. J. Biol. Macromol. 93 (2016) 1111–1117, https://doi.org/10.1016/j.ijbiomac.2016.09.066.

[27] C. Songsiriritthigul, S. Pantoom, A.H. Aguda, R.C. Robinson, W. Suginta, Crystal structures of *Vibrio harveyi* chitinase a complexed with chitooligosaccharides: implications for the catalytic mechanism, J. Struct. Biol. 162 (2008) 491–499, https://doi.org/10.1016/j.jsb.2008.03.008.

[28] S.A. Hollingsworth, R.O. Dror, Molecular dynamics simulation for all, Neuron 99 (2018) 1129–1143, https://doi.org/10.1016/j.neuron.2018.08.011.

[29] A. Segura-Cabrera, V. Bocanegra-García, C. Lizarazo-Ortega, X. Guo, J. Correa-Basurto, M.A. Rodríguez-Pérez, A computational analysis of the binding mode of closantel as inhibitor of the *Onchocerca volvulus* chitinase: insights on macrofilaricidal drug design, J. Comput. Aided Mol. Des. 25 (2011) 1107–1119, https://doi.org/10.1007/s10822-011-9489-y.

[30] F.I. Khan, A. Govender, K. Permaul, S. Singh, K. Bisetty, Thermostable chitinase II from *Thermomyces lanuginosus* SSBP: cloning, structure prediction and molecular dynamics simulations, J. Theor. Biol. 374 (2015) 107–114, https://doi.org/10.1016/j.jtbi.2015.03.035.

[31] F.I. Khan, K. Bisetty, D.Q. Wei, M.I. Hassan, A pH based molecular dynamics simulations of chitinase II isolated from *Thermomyces lanuginosus* SSBP, Cogent. Biol. 2 (2016) 1168336, https://doi.org/10.1080/23312025.2016.1168336.

[32] F.I. Khan, K. Bisetty, K.R. Gu, S. Singh, K. Permaul, M.I. Hassan, D.Q. Wei, Molecular dynamics simulation of chitinase I from *Thermomyces lanuginosus SSBP* to ensure optimal activity, Mol. Simul. 43 (2017) 480–490, https://doi.org/10.1080/08927022.2016.1237024.

[33] J. Jitonnom, M.A.L. Limb, A.J. Mulholland, QM/MM free-energy simulations of reaction in *Serratia marcescens* chitinase B reveal the protonation state of Asp142 and the critical role of Tyr214, J. Phys. Chem. B 118 (2014) 4771–4783, https://doi.org/10.1021/jp500652x.

[34] I. Incir, O. Kaplan, *Escherichia coli* as a versatile cell factory: advances and challenges in recombinant protein production, Protein Expr. Purif. 219 (2024) 106463, https://doi.org/10.1016/j.pep.2024.106463.
[35] A. Beygmoradi, A. Homaei, R. Hemmati, P. Fernandes, Recombinant protein expression: challenges in production and folding related matters, Int. J. Biol. Macromol. 233 (2023) 123407, https://doi.org/10.1016/j.ijbiomac.2023.123407.
[36] A. Bateman, M.J. Martin, S. Orchard, M. Magrane, S. Ahmad, E. Alpi, E. H. Bowler-Barnett, UniProt: the universal protein knowledgebase in 2023, Nucleic Acids Res. 51 (D1) (2023) D523–D531, https://doi.org/10.1093/nar/gkac1052.
[37] J. Sambrook, D.W. Russell, Preparation and transformation of competent *E. coli* using calcium chloride, CSH Protoc. 2006 (1) (2006) pdb-prot3932, https://doi.org/10.1101/pdb.prot3932.
[38] V. Govindaraj, S.K. Kim, R. Raval, K. Raval, Marine *Bacillus haynesii* chitinase: purification, characterization, and antifungal potential for sustainable chitin bioconversion, Carbohydr. Res. (2024) 109170, https://doi.org/10.1016/j.carres.2024.109170.
[39] W.S. Abbott, A method of computing the effectiveness of an insecticide, J. Econ. Entomol. 18 (1925) 265–267.
[40] A. Waterhouse, M. Bertoni, S. Bienert, G. Studer, G. Tauriello, R. Gumienny, F. T. Heer, T.A.P. de Beer, C. Rempfer, L. Bordoli, R. Lepore, T. Schwede, SWISS-MODEL: homology modelling of protein structures and complexes, Nucleic Acids Res. 46 (2018) W296–W303, https://doi.org/10.1093/nar/gky427.
[41] H.M. Berman, J. Westbrook, Z. Feng, G. Gilliland, T.N. Bhat, H. Weissig, I. V. Shindyalov, P.E. Bourne, The protein data bank, Nucleic Acids Res. 28 (2000) 235–242, https://doi.org/10.1093/nar/28.1.235.
[42] G. Studer, G. Tauriello, S. Bienert, M. Biasini, N. Johner, T. Schwede, ProMod3—a versatile homology modelling toolbox, PLoS Comput. Biol. 17 (2021) e1008667, https://doi.org/10.1371/journal.pcbi.1008667.
[43] M. Bertoni, F. Kiefer, M. Biasini, L. Bordoli, T. Schwede, Modeling protein quaternary structure of homo-and hetero-oligomers beyond binary interactions by homology, Sci. Rep. 7 (2017) 10480, https://doi.org/10.1038/s41598-017-09654-8.
[44] G. Studer, C. Rempfer, A.M. Waterhouse, R. Gumienny, J. Haas, T. Schwede, QMEANDisCo—distance constraints applied on model quality estimation, Bioinformatics 36 (2020) 1765–1771, https://doi.org/10.1093/bioinformatics/btz828.
[45] S.C. Lovell, I.W. Davis, W.B. Arendall, P.I. De Bakker, J.M. Word, M.G. Prisant, J. S. Richardson, D.C. Richardson, Structure validation by cα geometry: ϕ, ψ and cβ deviation, Proteins 50 (2003) 437–450, https://doi.org/10.1002/prot.10286.
[46] E.F. Pettersen, T.D. Goddard, C.C. Huang, G.S. Couch, D.M. Greenblatt, E. C. Meng, T.E. Ferrin, UCSF chimera—a visualization system for exploratory research and analysis, J. Comput. Chem. 25 (2004) 1605–1612, https://doi.org/10.1002/jcc.20084.
[47] O. Trott, A. Olson, Software news and update autodock vina: improving the speed and accuracy of docking with a new scoring function, J. Comput. Chem. 31 (2009) 455–461, https://doi.org/10.1002/jcc.21334.
[48] J. Eberhardt, D. Santos-Martins, A.F. Tillack, S. Forli, AutoDock Vina 1.2.0: new docking methods, expanded force field, and python bindings, J. Chem. Inf. Model. 61 (2021) 3891–3898, https://doi.org/10.1021/acs.jcim.1c00203.
[49] M.F. Adasme, K.L. Linnemann, S.N. Bolz, F. Kaiser, S. Salentin, V.J. Haupt, M. Schroeder, PLIP 2021: Expanding the scope of the protein–ligand interaction profiler to DNA and RNA, Nucleic Acids Res. 49 (2021) W530–W534, https://doi.org/10.1093/nar/gkab294.
[50] S. Jo, T. Kim, V.G. Iyer, W. Im, CHARMM-GUI: a web-based graphical user interface for CHARMM, J. Comput. Chem. 29 (11) (2008) 1859–1865, https://doi.org/10.1002/jcc.20945.
[51] J. Lee, X. Cheng, S. Jo, A.D. MacKerell, J.B. Klauda, W. Im, CHARMM-GUI input generator for NAMD, GROMACS, AMBER, OpenMM, and CHARMM/OpenMM simulations using the CHARMM36 additive force field, Biophys. J. 110 (3) (2016) 641a.
[52] V. Zoete, M.A. Cuendet, A. Grosdidier, O. Michielin, SwissParam: a fast force field generation tool for small organic molecules, J. Comput. Chem. 32 (2011) 2359–2368, https://doi.org/10.1002/jcc.21816.
[53] M. Bugnon, M. Goullieux, U.F. Röhrig, M.A. Perez, A. Daina, O. Michielin, V. Zoete, SwissParam, A modern web-based tool for efficient small molecule parametrization, J. Chem. Inf. Model. 63 (2023) (2023) 6469–6475, https://doi.org/10.1021/acs.jcim.3c01053.
[54] J.C. Phillips, R. Braun, W. Wang, J. Gumbart, E. Tajkhorshid, E. Villa, C. Chipot, R.D. Skeel, L. Kalé, K. Schulten, Scalable molecular dynamics with NAMD, J. Comput. Chem. 26 (2005) 1781–1802, https://doi.org/10.1002/jcc.20289.
[55] J.C. Phillips, D.J. Hardy, J.D. Maia, J.E. Stone, J.V. Ribeiro, R.C. Bernardi, R. Buch, G. Fiorin, J. Hénin, W. Jiang, R. McGreevy, M.C.R. Melo, B.K. Radak, R. D. Skeel, A. Singharoy, Y. Wang, B. Roux, A. Aksimentiev, Z. Luthey-Schulten, L. V. Kalé, K. Schulten, C. Chipot, E. Tajkhorshid, Scalable molecular dynamics on CPU and GPU architectures with NAMD, J. Chem. Phys. 153 (4) (2020) 044130, https://doi.org/10.1063/5.0014475.
[56] W. Humphrey, A. Dalke, K. Schulten, VMD: visual molecular dynamics, J. Mol. Graph. 14 (1996) 33–38, https://doi.org/10.1016/0263-7855(96)00018-5.
[57] R. Thomas, T. Fukamizo, W. Suginta, Bioeconomic production of high-quality chitobiose from chitin food wastes using an in-house chitinase from *Vibrio campbellii*, Bioresour. Bioprocess. 9 (2022) 86, https://doi.org/10.1186/s40643-022-00574-8.
[58] Q. Zhang, X. Zhang, Y. He, Y. Li, The synergistic action of two chitinases from Vibrio harveyi on chitin degradation, Carbohydr. Polym. 307 (2023) 120640, https://doi.org/10.1016/j.carbpol.2023.120640.
[59] J. Li, J. Zheng, Y. Liang, R. Yan, X. Xu, J. Lin, Expression and characterization of a chitinase from *Serratia marcescens*, Protein Expr. Purif. 171 (2020) 105613, https://doi.org/10.1016/j.pep.2020.105613.
[60] C. Lv, T. Gu, R. Ma, W. Yao, Y. Huang, J. Gu, G. Zhao, Biochemical characterization of a GH19 chitinase from *Streptomyces alfalfae* and its applications in crystalline chitin conversion and biocontrol, Int. J. Biol. Macromol. 167 (2021) 193–201, https://doi.org/10.1016/j.ijbiomac.2020.11.178.
[61] X. Qin, Y. Xin, X. Su, X. Wang, J. Zhang, T. Tu, Y. Wang, B. Yao, H. Huang, H. Luo, Heterologous expression and characterization of thermostable chitinase and β-N-acetylhexosaminidase from *Caldicellulosiruptor acetigenus* and their synergistic action on the bioconversion of chitin into N-acetyl-d-glucosamine, Int. J. Biol. Macromol. 192 (2021) 250–257, https://doi.org/10.1016/j.ijbiomac.2021.09.204.
[62] L. Ran, X. Wang, X. He, R. Guo, Y. Wu, P. Zhang, X.H. Zhang, Genomic analysis and chitinase characterization of *Vibrio harveyi* WXL538: insight into its adaptation to the marine environment, Front. Microbiol. 14 (2023) 1121720, https://doi.org/10.3389/fmicb.2023.1121720.
[63] Y. Yu, S. Chen, M. Yan, Y. Li, M. Yang, X. Liu, J. Miao, X. Wang, M. Xiao, H. Mou, K. Leng, Identification, expression, and characterization of a marine-derived chitinase Ce0303 from *Chitiniphilus eburneus* YS-30 with exo-and endo-hydrolytic properties, Int. J. Biol. Macromol. 276 (2024) 133980, https://doi.org/10.1016/j.ijbiomac.2024.133980.
[64] X. He, M. Yu, Y. Wu, L. Ran, W. Liu, X.H. Zhang, Two highly similar chitinases from marine *Vibrio* species have different enzymatic properties, Mar. Drugs 18 (2020) 139, https://doi.org/10.3390/md18030139.
[65] B. Essghaier, M. Zouaoui, A. Najjari, N. Sadfi, Potentialities and characterization of an antifungal chitinase produced by a halotolerant *Bacillus licheniformis*, Curr. Microbiol. 78 (2021) 513–521, https://doi.org/10.1007/s00284-020-02329-0.
[66] R. Kumari, M. Kumar, P.K. Dadheech, V. Vivekanand, N. Pareek, Response surface optimization, purification, characterization and short-chain chitooligosaccharides production from an acidic, thermostable chitinase from *Thermomyces dupontii*, Int. J. Biol. Macromol. 267 (2024) 131362, https://doi.org/10.1016/j.ijbiomac.2024.131362.
[67] S.H. Park, J.H. Lee, H.K. Lee, Purification and characterization of chitinase from a marine bacterium, *Vibrio* sp. 98CJ11027, J. Microbiol. 38 (2000) 224–229.
[68] Y.T. Wang, P.L. Wu, Gene cloning, characterization, and molecular simulations of a novel recombinant chitinase from *Chitinibacter Tainanensis* CT01 appropriate for chitin enzymatic hydrolysis, Polymers 12 (2020) 1648, https://doi.org/10.3390/polym12081648.
[69] Z. Ma, J. Tong, Y. Wang, Z. Zhou, Isolation and characterization of a thermostable alkaline chitinase-producing *Aeromonas* strain and its potential in biodegradation of shrimp shell wastes, Rom Biotechnol Lett 26 (2021) 2511–2522, https://doi.org/10.25083/rbl/26.2/2511.2522.
[70] S.S. Behera, S. Nivedita, H.T. Behera, L. Ray, Partial purification and characterization of an extracellular chitin deacetylase from *Streptomyces griseoincarnatus* RB7AG isolated from Chilika lake, Microbe 1 (2023) 100020, https://doi.org/10.1016/j.microb.2023.100020.
[71] Y. Liu, G. Sun, J. Liu, Y. Lou, J. Zhu, C. Wang, Enzymatic production of diverse N-acetyl chitooligosaccharides employing a novel bifunctional chitinase and its engineered variants, Food Chem. 453 (2024) 139675, https://doi.org/10.1016/j.foodchem.2024.139675.
[72] K. Rajendran, M. Krishnamoorthy, K. Karuppiah, K. Ethiraj, S. Sekar, Chitinase from *Streptomyces mutabilis* as an effective eco-friendly biocontrol agent, Appl. Biochem. Biotechnol. 196 (2024) 18–31, https://doi.org/10.1007/s12010-023-04489-8.
[73] U. Jankiewicz, B. Baranowski, M. Swiontek Brzezinska, M. Frąk, Purification, characterization and cloning of a chitinase from Stenotrophomonas rhizophila G22, 3, Biotech 10 (2020) 1–10, https://doi.org/10.1007/s13205-019-2007-y.
[74] K. Dwyer, I.S. Bentley, D.A. Fitzpatrick, A.A. Saleh, E. Tighe, E. McGleenan, G. Darragh, G. Walsh, Recombinant production, characterization and industrial application testing of a novel acidic exo/endo-chitinase from *Rasamsonia emersonii*, Extremophiles 27 (2023) 10, https://doi.org/10.1007/s00792-023-01293-4.
[75] L. Ray, A.N. Panda, S.R. Mishra, A.K. Pattanaik, T.K. Adhya, M. Suar, V. Raina, Purification and characterization of an extracellular thermo-alkali stable, metal tolerant chitinase from *Streptomyces chilikensis* RC1830 isolated from a brackish water lake sediment, Biotechnol Rep 21 (2019) e00311, https://doi.org/10.1016/j.btre.2019.e00311.
[76] J. Du, S. Duan, J. Miao, M. Zhai, Y. Cao, Purification and characterization of chitinase from *Paenibacillus* sp, Biotechnol. Appl. Biochem. 68 (2021) 30–40, https://doi.org/10.1002/bab.1889.
[77] X.H. Xie, X. Fu, X.Y. Yan, W.F. Peng, L.X. Kang, A broad-specificity chitinase from *Penicillium oxalicum* k10 exhibits antifungal activity and biodegradation properties of chitin, Mar. Drugs 19 (2021) 356, https://doi.org/10.3390/md19070356.
[78] N. Suryawanshi, J.S. Eswari, Purification and characterization of chitinase produced by thermophilic fungi *Thermomyces lanuginosus*, Prep. Biochem. Biotechnol. 52 (2022) 1087–1095, https://doi.org/10.1080/10826068.2022.2028639.
[79] N. Thakur, A.K. Nath, A. Chauhan, R. Gupta, Purification, characterization, and antifungal activity of *Bacillus cereus* strain NK91 chitinase from rhizospheric soil

samples of Himachal Pradesh, India, Biotechnol. Appl. Biochem. 69 (2022) 1830–1842, https://doi.org/10.1002/bab.2250.
[80] C. Aktas, D. Ruzgar, S. Gurkok, A. Gormez, Purification and characterization of *Stenotrophomonas maltophilia* chitinase with antifungal and insecticidal properties, Prep. Biochem. Biotechnol. 53 (2023) 797–806, https://doi.org/10.1080/10826068.2022.2142942.
[81] Z. Ding, T. Li, M. Chen, Y. Fang, X. Hou, G. Yang, J. Lu, Q. Ye, R. Zhu, F. He, M. Xia, S. Liu, Purification and characterization of a chitinase from *Aeromonas media* CZW001 as a biocatalyst for producing chitinpentaose and chitinhexaose, Biotechnol. Appl. Biochem. 70 (2023) 281–289, https://doi.org/10.1002/bab.2351.
[82] C. Jiang, L. Li, J. Li, A novel antifungal chitinase from *Chaetomium globosum*: column-free purification and characterization, Arch. Microbiol. 207 (2025) 92, https://doi.org/10.1007/s00203-025-04295-2.
[83] C. Gu, J. Chen, X. Huang, Y. Jiang, N. Ou, D. Yang, M. Jiang, L. Pan, The impact of Chitinase binding domain truncation on the properties of ca Chi18B from *Chitinilyticum aquatile* CSC-1, Mar. Drugs 23 (2025) 93, https://doi.org/10.3390/md23030093.
[84] R. Singh, S.K. Upadhyay, M. Singh, I. Sharma, P. Sharma, P. Kamboj, A. Saini, R. Voraha, A.K. Sharma, T.K. Upadhyay, F. Khan, Chitin, chitinases and chitin derivatives in biopharmaceutical, agricultural and environmental perspective, Biointerface Res Appl Chem 11 (2021) 9985–10005, https://doi.org/10.33263/BRIAC113.998510005.
[85] M. Kumar, H. Chakdar, K. Pandiyan, S. Thapa, M. Shahid, A. Singh, A. K. Srivastava, A.K. Saxena, Bacterial chitinases: genetics, engineering and applications, World J. Microbiol. Biotechnol. 38 (2022) 252, https://doi.org/10.1007/s11274-022-03444-9.
[86] N.P. Dhole, M.A. Dar, R.S. Pandit, Recent advances in the bioprospection and applications of chitinolytic bacteria for valorization of waste chitin, Arch. Microbiol. 203 (2021) 1953–1969.
[87] U. Dave, E. Somanader, P. Baharlouei, L. Pham, M.A. Rahman, Applications of chitin in medical, environmental, and agricultural industries, J Mar Sci Eng 9 (2021) 1173, https://doi.org/10.3390/jmse9111173.
[88] J. Han, M. Ullah, V. Andoh, M.N. Khan, Y. Feng, Z. Guo, H. Chen, Engineering bacterial chitinases for industrial application: from protein engineering to bacterial strains mutation! a comprehensive review of physical, molecular, and computational approaches, J. Agric. Food Chem. 72 (2024) 23082–23096, https://doi.org/10.1021/acs.jafc.4c06856.
[89] B. He, L. Yang, D. Yang, M. Jiang, C. Ling, H. Chen, F. Ji, L. Pan, Biochemical purification and characterization of a truncated acidic, thermostable chitinase from marine fungus for N-acetylglucosamine production, Front. Bioeng. Biotechnol. 10 (2022) 1013313, https://doi.org/10.3389/fbioe.2022.1013313.
[90] H. Mali, C. Shah, B.H. Raghunandan, A.S. Prajapati, D.H. Patel, U. Trivedi, R. B. Subramanian, Organophosphate pesticides an emerging environmental contaminant: pollution, toxicity, bioremediation progress, and remaining challenges, J. Environ. Sci. 127 (2023) 234–250, https://doi.org/10.1016/j.jes.2022.04.023.
[91] Y. Nikmanesh, M. Farhadi, M. Taherian, P. Asban, F. Kiani, M.J. Mohammadi, The health endpoint due to exposure organophosphorus toxicant, Clin. Epidemiol. Glob. Health 25 (2024) 101508, https://doi.org/10.1016/j.cegh.2024.101508.
[92] H. Laribi-Habchi, K. Bouacem, F. Allala, F. Jabeur, O. Selama, S. Mechri, M. Yahiaoui, A. Bouanane-Darenfed, B. Jaouadi, Characterization of chitinase from *Shewanella inventionis* HE3 with bio-insecticidal effect against granary weevil, *Sitophilus granarius* Linnaeus (Coleoptera: *Curculionidae*), Process Biochem. 97 (2020) 222–233, https://doi.org/10.1016/j.procbio.2020.06.023.
[93] F. Berini, A. Montali, R. Liguori, G. Venturini, M. Bonelli, L. Shaltiel-Harpaz, M. Reguzzoni, M. Siti, F. Marinelli, M. Casartelli, G. Tettamanti, Production and characterization of *Trichoderma asperellum* chitinases and their use in synergy with *Bacillus thuringiensis* for lepidopteran control, Pest Manag. Sci. 80 (2024) 3401–3411, https://doi.org/10.1002/ps.8045.
[94] N. Karki, A.U. Paschapur, A.R. Subbanna, J. Stanley, A.K. Singh, I. Bisht, J. P. Gupta, Identification and characterization of chitinase-producing bacteria from gut of pleurostict scarab beetle grubs (Coleoptera: Scarabaeidae), Int. J. Trop. Insect. Sci. 43 (2023) 1539–1551, https://doi.org/10.1007/s42690-023-01049-9.
[95] F.M. Tawfiq, F.E.Z.A. Abd El, S.H. Salem, A.M. Elshahawy, A.M. Sayed, A. A. Abdel-Hafez, Enhanced biological activity of chitinase immobilized on cobalt metal-organic framework: isolation, characterization, and potential applications, Int. J. Biol. Macromol. 308 (2025) 142538, https://doi.org/10.1016/j.ijbiomac.2025.142538.
[96] A.K. Singh, A. Singh, P. Joshi, Combined application of chitinolytic bacterium *Paenibacillus* sp. d1 with low doses of chemical pesticides for better control of *Helicoverpa armigera*, Int. J. Pest Manag. 62 (2016) 222–227, https://doi.org/10.1080/09670874.2016.1167267.
[97] U. Azizoglu, G. Salehi Jouzani, E. Sansinenea, V. Sanchis-Borja, Biotechnological advances in *Bacillus thuringiensis* and its toxins: recent updates, Rev. Environ. Sci. Biotechnol. 22 (2023) 319–348, https://doi.org/10.1007/s11157-023-09652-5.
[98] M. Biasini, S. Bienert, A. Waterhouse, K. Arnold, G. Studer, T. Schmidt, F. Kiefer, T.G. Cassarino, M. Bertoni, L. Bordoli, T. Schwede, SWISS-MODEL: modelling protein tertiary and quaternary structure using evolutionary information, Nucleic Acids Res. 42 (2014) W252–W258, https://doi.org/10.1093/nar/gku340.
[99] L.R. Forrest, C.L. Tang, B. Honig, On the accuracy of homology modeling and sequence alignment methods applied to membrane proteins, Biophys. J. 91 (2006) 508–517, https://doi.org/10.1529/biophysj.106.082313.
[100] Z. Xiang, Advances in homology protein structure modeling, Curr. Protein Pept. Sci. 7 (2006) 217–227, https://doi.org/10.2174/138920306777452312.
[101] P. Benkert, M. Biasini, T. Schwede, Toward the estimation of the absolute quality of individual protein structure models, Bioinformatics 27 (2011) 343–350, https://doi.org/10.1093/bioinformatics/btq662.
[102] D.M.F. Van Aalten, B. Synstad, M.B. Brurberg, E. Hough, B.W. Riise, V.G. H. Eijsink, R.K. Wierenga, Structure of a two-domain chitotriosidase from *Serratia marcescens* at 1.9-Å resolution, Proc. Natl. Acad. Sci. USA 97 (2000) 5842–5847, https://doi.org/10.1073/pnas.97.11.5842.
[103] A. Perrakis, I. Tews, Z. Dauter, A.B. Oppenheim, I. Chet, K.S. Wilson, C.E. Vorgias, Crystal structure of a bacterial chitinase at 2.3 Å resolution, Structure 2 (1994) 1169–1180.